Experimental database of mixed-mode crack propagation tests performed on mortar specimens with a hexapod and full-field measurements.
Part II: interactive loading

A. Carpiuc-Prisacari[a,b,c], C. Jailin[a], M. Poncelet[a,*], K. Kazymyrenko[b,c], H. Leclerc[a], F. Hild[a]

[a]LMT (ENS Paris-Saclay / CNRS / Université Paris-Saclay)
61 avenue du Président Wilson, 94235 Cachan Cedex, France
[b]IMSIA, UMR EDF-CNRS-CEA-ENSTA 9219 Université Paris-Saclay
828 Boulevard des Maréchaux, 91762 Palaiseau Cedex, France
[c]EDF Lab Paris-Saclay, 7 boulevard Gaspard Monge, 91120 Palaiseau, France

Abstract

This second paper presents a series of 4 crack propagation tests with the same experimental protocol as in a companion paper, but with some significant loading modifications. The first difference is that the loading is composed of in-plane rotation in addition to tension and shear translations. The second difference is that the loading is manually changed during the tests, depending on the crack tip location. This leads to tests with several bifurcations, and/or different loading ratios during the same test. One of them leads to mode I+II, and then mode I+III crack propagation. Some tests end with instabilities while others are controlled to be stable up to the complete failure of the specimen. In some cases, crack closure and friction between the crack faces occur.

Keywords: Crack propagation, Digital Image Correlation, Mixed-mode fracture, Mortar, Multiaxial tests

*A. Carpiuc-Prisacari
Email address: `andreea.carpiuc@edf.fr` (A. Carpiuc-Prisacari)

1. Introduction

In a companion paper proportional and non-proportional crack propagation tests were performed on mortar specimens [1]. The experimental protocol is a modern version of the so-called Nooru-Mohamed tests [2, 3]. While keeping the same specimen geometry and loading types (Fig. 1(a-b)), the testing machine and the measurement techniques were improved. Contrary to other tests found in the literature [4, 5, 6, 7, 8, 9, 10, 11, 12, 13, 14, 2], these experiments were conducted with an experimental protocol combining two main features, namely, the loading history was applied with a hexapod [15, 16], and the displacement fields on both faces of the samples were measured via Digital Image Correlation (DIC) [17].
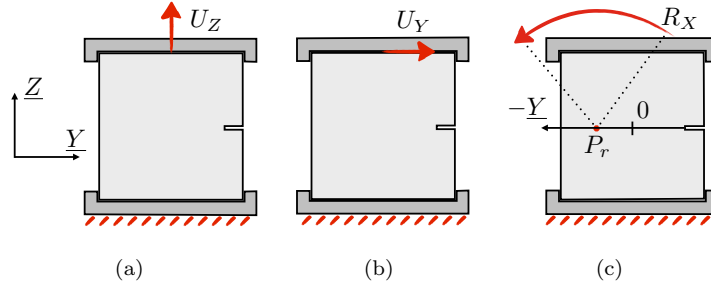

Figure 1: Different loading histories. Global in-plane tension U_Z (a), shear U_Y (b) and rotation R_X about a point of horizontal coordinate P_r (c). The orientation of the axis for the coordinate of P_r is inverted ($-\underline{Y}$ instead of $\underline{Y}$) to have increasing values of P_r during the tests, since P_r is moved away from the crack tip to control its propagation.

The main conclusions of this first series of tests were:

- It was possible to accurately conduct tests on such a testing machine.

- Tests were repeatable at the global level.

- Mean force / mean displacement curves were consistent for identical test conditions, and in good agreement with the crack propagation scenario of each test.

2

- In the case of proportional loading histories, DIC results were in good agreement with the final crack pattern.

₂₀ - These tests, close to the Nooru-Mohamed configurations, shed new light on their interpretations.

However, there were some shortcomings:

- The period of stability of crack propagation was rather limited (*i.e.,* few millimeters to centimeters). Consequently, the 'period of interest' was
₂₅ short for each test.

- Final cracks were straight, *i.e.,* no reorientation occurred. It would be interesting to perform discriminating and sensitive tests to such reorientations. The Stress Intensity Factor (SIF) ratio $\frac{K_{II}}{K_I}$ thus was very limited during the stable propagation period.

₃₀ - As previously observed [18] on similar specimens and loading paths, the crack propagation differed on the surface and in the bulk of the sample. It was confirmed [1], since the DIC results were not representative of the cracks in the material bulk for non-proportional loadings. Therefore, a detailed comparison of the propagation regime between experimental and
₃₅ numerical results is expected to be more difficult to perform.

To circumvent these limitations, two important changes are proposed in this paper. First, in addition to the global tension (U_Z) and shear (U_Y) displacements that characterize the previous tests, an in-plane rotation (R_X) was added (Fig. 1(c)) with controlled positions of the instantaneous center of rotation P_r.
₄₀ This rotational degree of freedom will induce a tensile (and/or compressive) stress gradient. Consequently, when the crack propagates the mode I SIF (K_I) will decrease and the propagation will possibly stop. It is even possible to have a part of the specimen under compression, thereby preventing any propagation or initiation in that region. Moreover, having a sufficiently heterogeneous stress
₄₅ field prevents surface cracks from initiating away from the notches. This technique is nothing more than the adaptation of the beam bending principle (where

<div align="center">3</div>

a stress gradient exists along the thickness of the beam, due to the moment induced by the forces applied at large distance) to a compact specimen case (*i.e.,* the rotation applied at short distance directly induces a moment).

Second, the prescribed loading history will be changed during the test, depending on the crack tip location. The latter can be assessed on the fly by DIC analyses as shown with the previously reported proportional loadings [1]. The SIF ratio that controls the crack orientation could be tuned by a combination of tension and shear. In the present case, the relationship between SIF and load applied on the boundaries is rather straightforward, namely, modifying the tensile level mainly changes the K_I value, while varying the shear level mainly changes K_{II}. This relationship is not exactly proportional, and depends on the crack tip location [19]. Yet this rule-of-thumb analysis enables the loading path to be chosen in advance to obtain a given crack path. One will then rely on the location of the crack tip during the test to modify the loading history in order to accurately obtain the sought result. Changing the loading conditions (*i.e.,* the SIF ratio) for a crack after non-negligible propagation is much more effective for crack reorientation investigations than changing the SIF ratio at the beginning of the test (as for non-proportional tests [1]). The very beginning of propagation is not representative of a fully formed crack since it evolves in a material affected by crack initiation and its interaction with the underlying material microstructure.

The paper will briefly describe the experimental protocol in a first part. Then the 4 so-called *interactive* tests will be described, and the test results will be analyzed.

2. Experimental setup

Most of the experimental setup is the same as in Ref. [1] with some minor modifications/additions. For a detailed description of the experimental protocol, which focuses on a given test of this campaign, see Ref. [20].

4

2.1. Testing machine

The testing device is a parallel machine composed of 6-axis electromechanical actuators, which are controlled in displacement mode. Its translation accuracy in the used conditions is about 1 μm [16]. The combination of a very slow displacement rate, the monitoring of the crack tip location (described thereafter) and the ability to stop and change the loading path during the test, leads to the possibility to control crack propagation so that a specific the crack path (*e.g.,* chevron, lightning bolt) is obtained.

2.2. Specimens

The specimens were $200 \times 200 \times 50$ mm rectangular parallelepipeds with different notches sawed at mid height of the sample (Fig. 2), namely, two notches (5×25 mm, or 5×40 mm) or only one (5×25 mm).
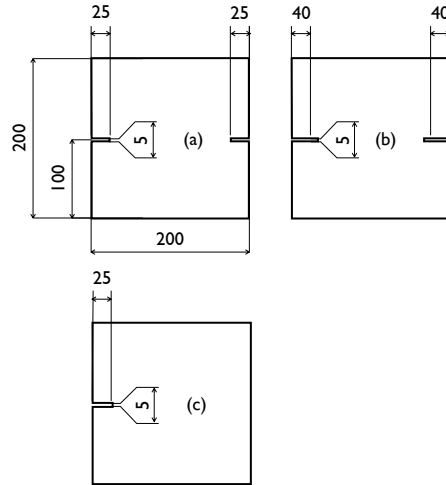

Figure 2: The 3 studied geometries with shallow double notches (a), deep double notches (b), and single shallow notch.

The samples were made of the same mortar (Table 1), casting and batch as in Ref. [1], and were stored in the same water basin with the other ones.

5

Table 1: Mortar mix details.

Effective water	Portland cement	Sand 0/4	Plasticizer
319 kg/m^3	611 kg/m^3	1235 kg/m^3	5.25 kg/m^3

The main mechanical properties of the mortar (Tab. 2) were obtained follow-
ing the NF EN 196-1 standard [21]. To check if the measured Young's modulus
was rate-dependent, 2 other specimens were tested with a load rate 100 times
lower, but no noticeable variation of Young's modulus or tensile strength oc-
curred. The standard compressive test NF EN 196-1 provided a strength equal
to 80 MPa. Last, the fracture energy G_f was obtained with 6 $70 \times 70 \times 280$ mm
specimens following the 50-FMC Draft Recommendation [22], and is equal to
115 ± 19 N/m.

Table 2: Average mortar properties obtained for two loading rate.

Load rate	Young modulus	Tensile strength
50 N/s	17.3 ± 0.7 GPa	3.8 ± 0.4 MPa
0.5 N/s	20.0 ± 0.1 GPa	4.1 ± 0.4 MPa

To perform the test reported hereafter, the specimens were glued to U-shaped
plates at the ends of the machine.

2.3. Displacement measurements

Full field kinematic measurements were performed during the test via digital
image correlation (DIC). Redundant macroscopic displacement measurements
obtained with a contact method (LVDT setup) were used to check the measure-
ment reliability.

2.3.1. 2D-DIC setup

2D-DIC was performed on each 200×200 mm face of the specimens with
2 2048×2048 pixel cameras, triggered every 5 s by a common TTL signal.

Regularized DIC [17] was used with 15 pixel-elements, and 250 pixel regularization length, which led to standard displacement uncertainties equal to 1.3 (resp. 2.4) μm along $\underline{Z}$ (resp. $\underline{Y}$) direction.

2.3.2. StereoDIC setup

A pair of cameras on each face was also used for (global) stereocorrelation [23, 24], thereby leading to a complete optical setup made of 6 cameras (Fig. 3). These additional 4 devices were 60D Canon Digital Single Lens Reflex cameras, equipped with F2.8 24-mm lenses. They were fixed on the same stiff aluminum frame (Newport, X95 series) as the other 2 cameras. All 6 cameras were synchronized. It was a low time-resolved measurement, yet compensated by views of the *whole* specimen glued onto the U-shaped plates.
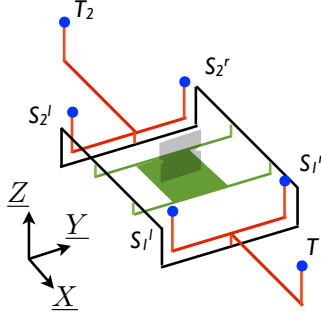
Figure 3: Location of the cameras with respect to the specimen: S_1^l & S_1^r , S_2^l & S_2^r for stereoDIC and T_1 and T_2 for 2D-DIC analyses.

The standard uncertainty of the rigid body motions between the upper and lower U-shaped plates obtained by stereocorrelation were assessed with 101 acquisitions when the hexapod was still. The values are 0.07 μm (resp. 0.68, 1.77) μm for a translation U_X (resp. U_Y, U_Z), and 3.6×10^{-4} rad (resp. 7.7×10^{-3}, 1.1×10^{-3}) for a rotation R_X (resp. R_Y, R_Z) [20].

2.3.3. Measurement redundancy

Six Linear Variable Differential Transducers (LVDT) were used, thereby providing a highly time-resolved measurement but with a limited spatial descrip-

tion, namely, only the 3 translations and 3 rotations applied to the upper part of the specimen are obtained. They however provided redundant information for the measurement of the rigid body motions of the boundaries. This configuration enabled the consistency of the measurement results to be checked since these two setups were completely independent (*i.e.,* 2 different measurement techniques and 2 separate frames).

The sensors were located close to the specimen, on the octogonal reference plate (Fig. 4). They were held by a rigid steel frame fixed on the lower plate, so that the relative displacement between the upper and the lower part of the machine were measured. The acquisition frequency was 10 Hz and their own standard uncertainty was 0.1 μm. As assessed in Ref. [20], the deviation of the LVDT setup is about 1 μm over a 2-mm range because of small biases (*e.g.,* misorientation of the octogonal plate, flatness defect).

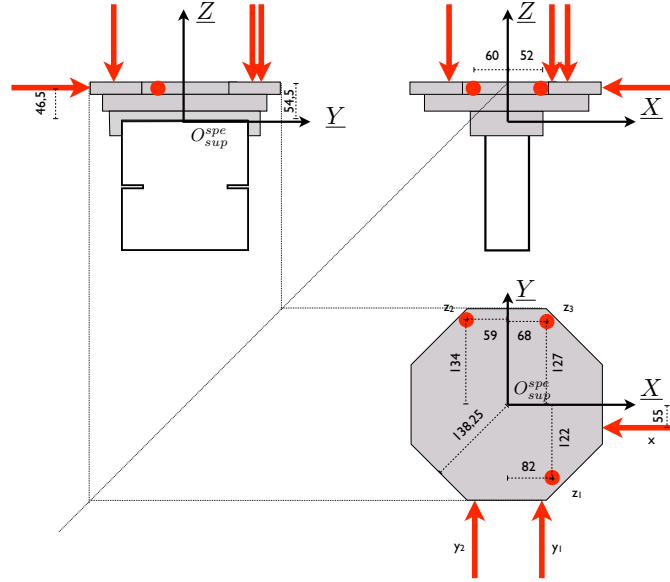

Figure 4: Location of the LVDT sensors with respect to the specimen.

8

3. Interactive tests

Based on the principle of adding an in-plane rotation R_X about a center of rotation P_r to ensure stability, 4 interactive tests $IT1$, $IT2$, $IT3$ and $IT4$ were performed. The instantaneous center of rotation was motionless (for $IT2$ and $IT4$ tests), or changed in a continuous way (for $IT3$ and $IT1$ test) or discretely (*i.e.,* beginning of $IT1$ test). Proportional and non-proportional propagations are also possible. One of the tests also ended with an out-of-plane loading. Each experiment aimed for specific propagation cases while sharing common features with others.

3.1. 2D boundary conditions

Various types of in-plane loading histories were selected:

- Single reorientation test ($IT1$). This test had both technical and scientific goals. From the technical point of view, it had to prove that the stabilization of crack propagation was possible, in addition to performing a clear reorientation after a first step of propagation (Fig. 5(a)). The loading path, schematically shown in Fig. 5(b), is simple. The first step is a proportional in-plane rotation (with the center of rotation P_r located at mid-width of the specimen, $P_r = 0$) with global shear in order to initiate and propagate a crack (1). The shear component is then slowly decreased to change its sign, so that the crack reorients (2). Last, the center of rotation P_r is progressively moved to the left, up to a location out of the specimen (*i.e.,* $P_r = 110$ mm, while the left boundary of the specimen is at 100 mm and the left notch at 75 mm) to resume propagation (3).
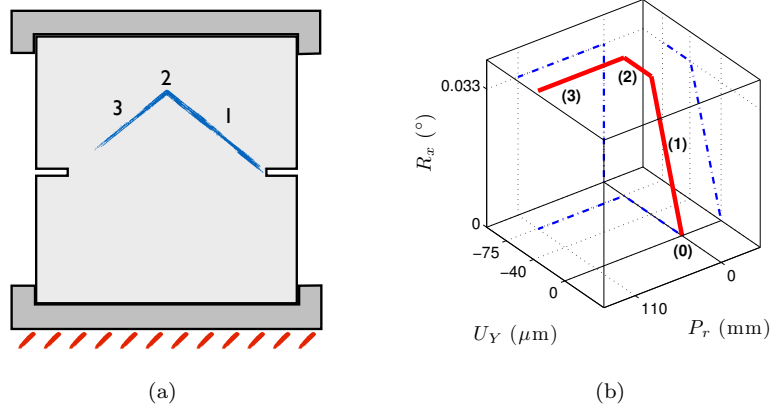
Figure 5: Single reorientation test $IT1$. Expected crack path (a) and corresponding loading path (b). P_r stands for the position along $\underline{Y}$ of the center of rotation.

From the scientific point of view, the data associated with *stable* crack propagation and reorientation are of interest. Friction of the crack mouth is possible after the first propagation step since the shear component in the opposite direction during the second step tends to close the part of the crack created during the first step.

- Crack link-up test ($IT2$). The technical interest of this test was to show that it was possible to *independently* initiate and propagate two cracks (Fig. 6(a)) by adjusting the in-plane rotation. A loading path consisting of two rotations of opposite sign, with their center of rotation P_r kept at 0, coupled with shear and then a final proportional tension-shear loading was applied (Fig. 6(b)).
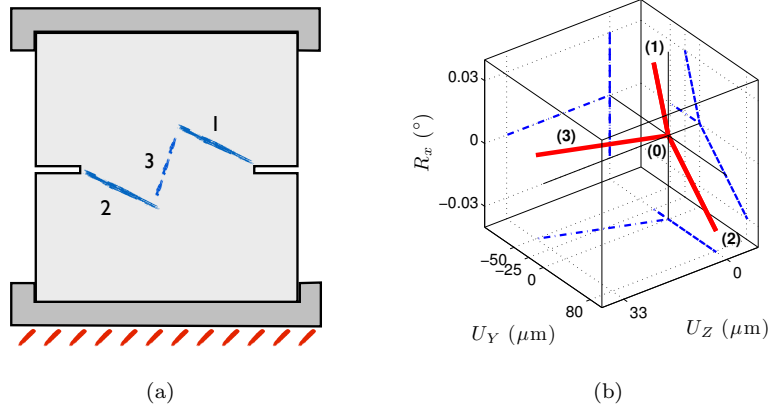
10

Figure 6: Single reorientation test $IT2$. Expected crack path (a) and corresponding loading path (b).

The scientific goal was to investigate crack closure since the first crack will be closed during the initiation of the second crack. The second point of interest was the link-up phenomenon appearing at the end of the test, when the two cracks initiating from each notch interacted and joined. The test was thus ended by a global tensile loading to force crack coalescence.

- Multiple reorientation test ($IT3$). By following the same principle as in test $IT1$ several times, several reorientations were expected (Fig. 7(a)). To ensure that the crack did not propagate too much at each step, different centers of rotation were considered (by increasing values of P_r, each time located farther away from the notch, see Fig. 7 (b)). Because several reorientations were expected, potential branchings might also appear. This test was thus interesting for investigating the branching/bifurcation conditions. It is thoroughly described in Ref. [20] and, as part of the whole test campaign, it will only be summarized herein.
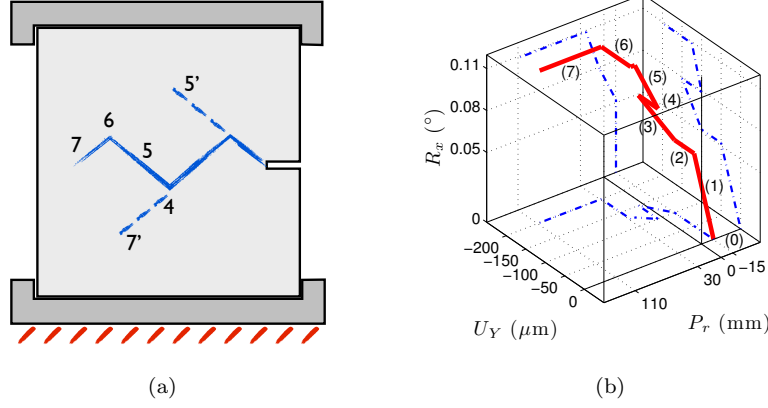
11

Figure 7: Multiple reorientation test $IT3$. Expected crack path (a) and corresponding loading path (b).

3.2. 3D boundary conditions

A first part of the $IT4$ test aimed at initiating and propagating a crack in mixed I+II mode. Shear (step $I-1$ in Fig. 8(a)) followed by in-plane rotation with shear (step $I-2$) was applied. The center of rotation was located at the center of the specimen ($P_r = 0$) to ensure that the crack does not propagate beyond this point. The specimen was then completely unloaded (step $I-3$). During the second part of the test, a rotation along the $\underline{Z}$ axis was applied to induce mode III propagation (step $II-1$ in Fig. 8 (b)). Last, a large translation along $\underline{Z}$ was applied (step $II-2$) to fully open the crack.
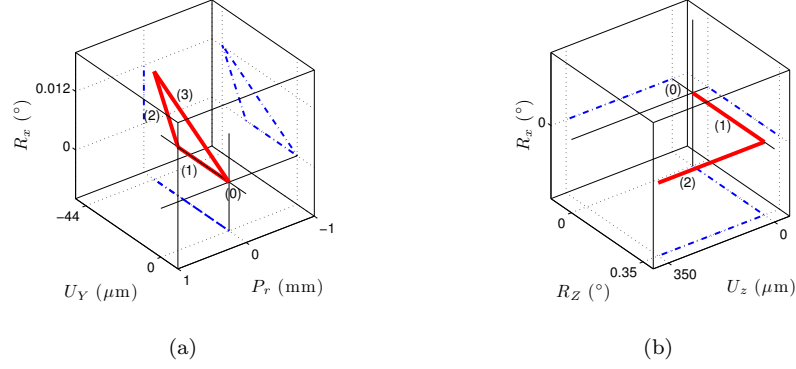
Figure 8: First (a) and second (b) loading steps of $IT4$ test.

The technical interest of this test was to show that the setup was also adapted for out-of-plane loadings inducing mode III propagation. The scientific interest is to perform a complex test with mode III propagation with crack closure/friction.

4. Test results

In this section the histories of forces and torques, and displacement fields will be presented and commented for each interactive test. Contrary to the previously reported results [1], forces and torques are no longer displayed as functions of the corresponding mean displacement (*e.g.*, $F_Z(U_Z)$) since the rotation contribution is not straightforward. For the sake of clarity, the forces and torques are plotted with respect to time.

4.1. Test IT1

Following the planned loading history depicted in Fig. 5, the final crack paths are shown in Figs. 10 and 11. As expected, they exhibit a chevron-like shape.

The load history was correctly followed by the machine (Fig. 9). The test started with an elastic loading-unloading ($[0 - 1, 400]$ s period), then the initiation-propagation stage was composed of three loading steps as planned

13

([1, 400 − 7, 200] s, [7, 200 − 14, 400] s and [14, 400 − 27, 000] s periods). An overall good agreement is observed between the mean relative displacements measured by LVDTs, DIC, and the control signal. Since very small values of U_X were measured and the out-of-plane loads F_X, M_Y and M_Z were close to zero, it is concluded that the test had no out-of-plane components.
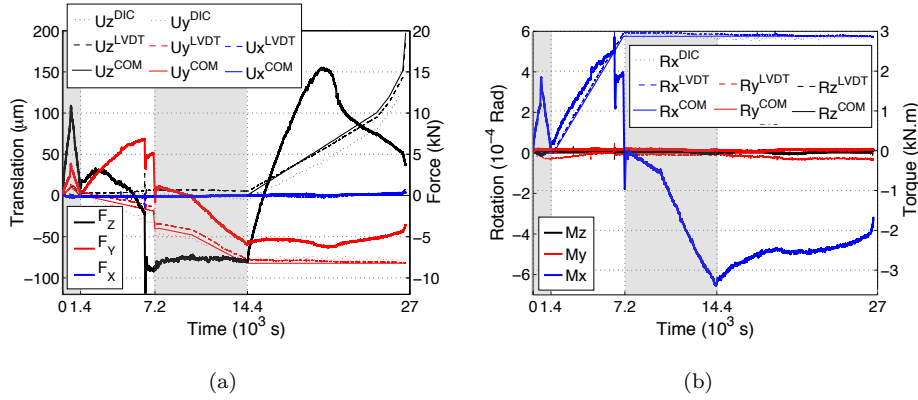

Figure 9: Translation and force vs. time (a). Rotation and torque vs. time (b) for $IT1$ test (steps are marked by white and light gray backgrounds).

Concerning propagation, several points are noteworthy. First, during step 1 consisting of a U_Y translation combined with an R_X rotation to initiate and propagate a crack toward the upper part of the sample, a sudden drop in F_Y, F_Z and M_X was observed. This was due to unstable propagation occurring between the instants labelled $1u$ and $1s$ in Figs. 10 and 11. This sudden propagation stopped because of the compression state previously prescribed ahead of the crack thanks to the R_X rotation. Second, the F_Y and M_X apparent drops at the beginning of the second step were on the contrary due to fast (yet controlled) shear unloading, not unstable propagation. Third, no propagation was observed during the entire step 2 while during step 3 (*i.e.,* the final U_Z translation), crack propagation was gradual. Last, the abrupt final failure occurred when the ligament was about 5 % of the specimen width.
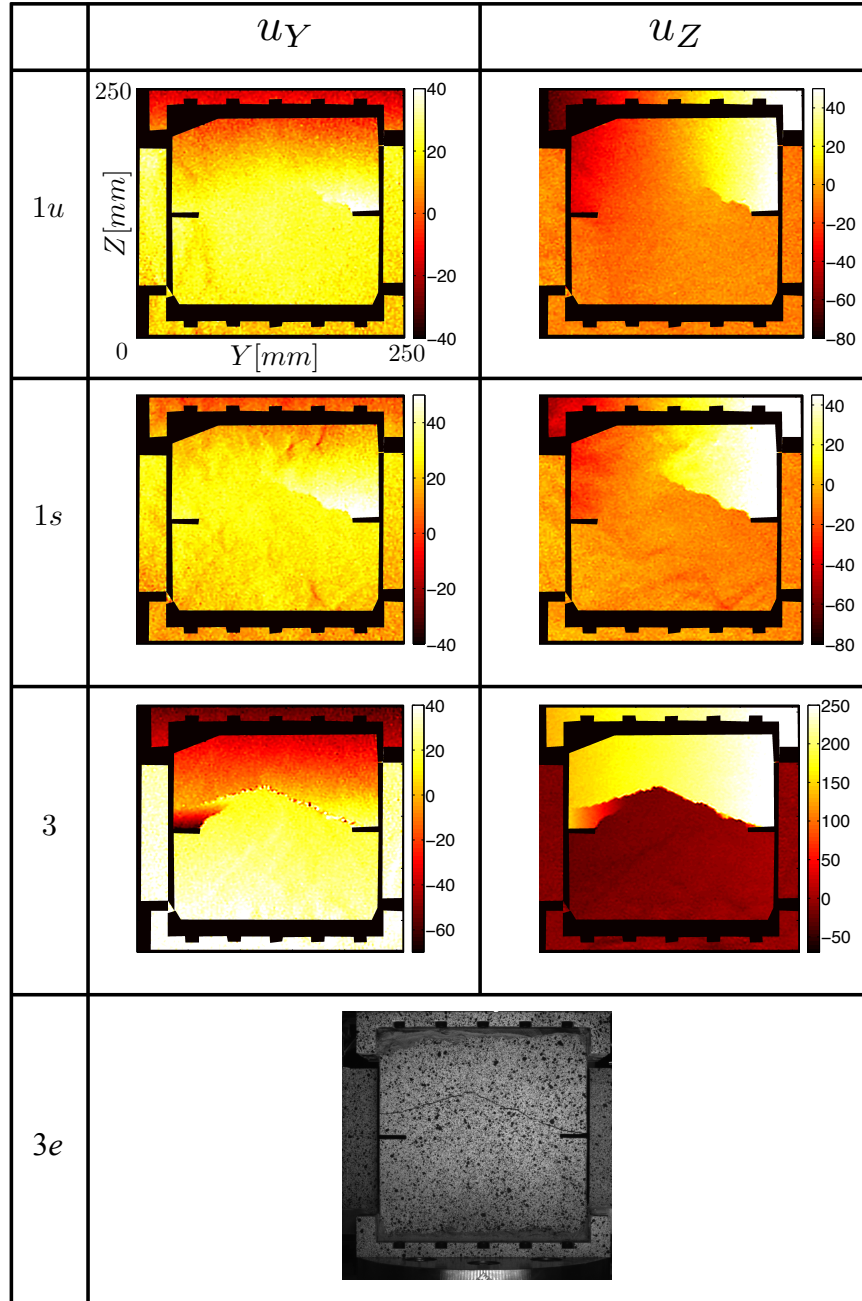
14

Figure 10: Displacement fields (expressed in μm) on face 1 just before unstable propagation during step 1 (1u) and next stable position (1s), and at the end of step 3 for test $IT1$.
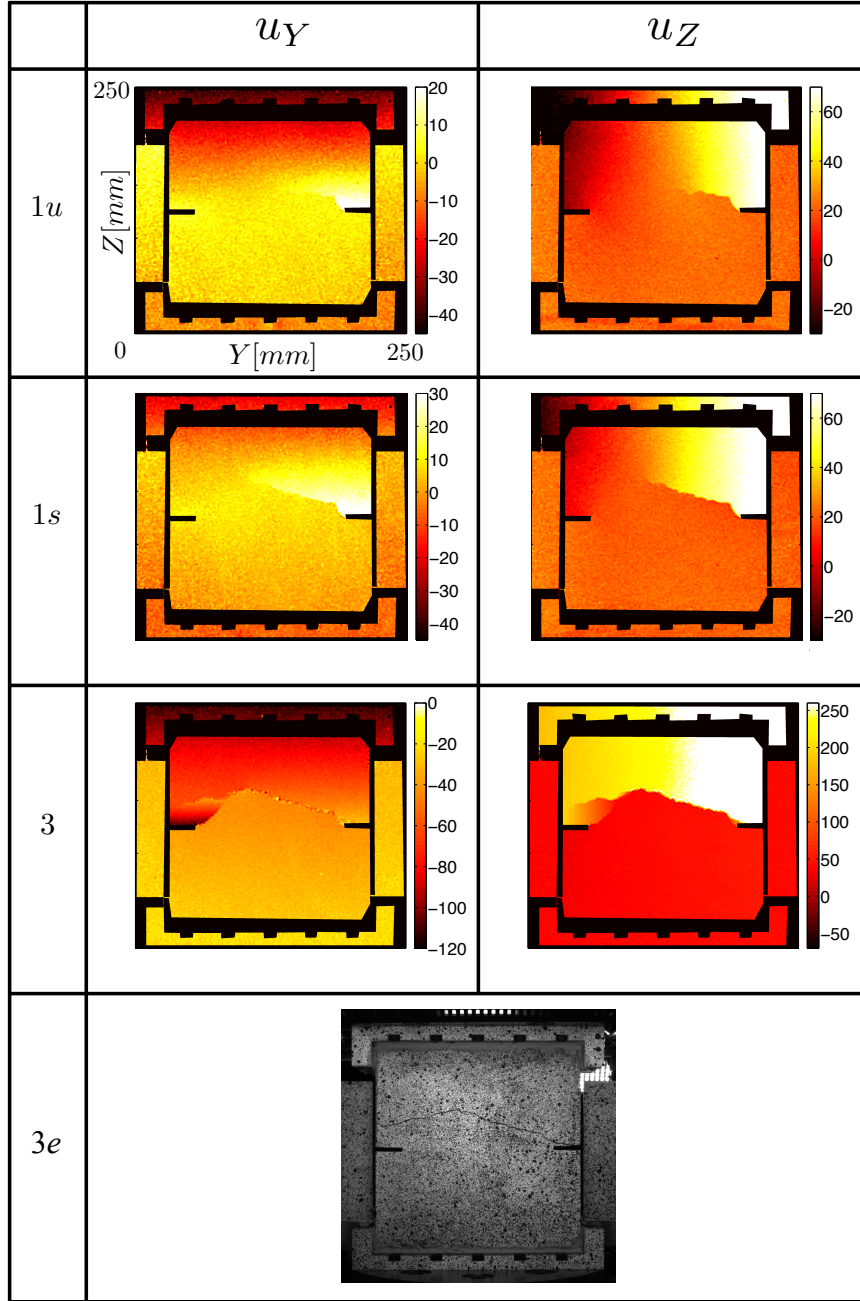
15

Figure 11: Displacement fields (expressed in μm) on face 2 just before unstable propagation during step 1 ($1u$) and next stable position ($1s$), and at the end of step 3 for test $IT1$. Face 2 images are flipped to make the comparison easier.

16

Concerning crack closure and friction, progressive softening was visible on F_Z and M_X curves during step 3, while the F_Y magnitude also decreased, albeit to a much lesser extent. This observation tends to prove that crack friction occurred, as well as the fact that the displacement field u_Y were continuous on some parts of the crack mouth at the end of the test (see Figs. 10 and 11). It is noteworthy that the sharp variation of slope at $t \approx 10,000$ s was only due to chosen changes in the control signal speed, not to crack closure. A last noticeable point was the appearance of a late second crack. It initiated from the second notch and slowly propagated. The first one did not seem to be influenced by the second crack, and propagated in a straight way. It thus seems reasonable to consider that this second crack is shallow.

4.2. Test IT2

By applying the planned loading history shown in Fig. 6, the crack paths shown in Figs. 13 and 14 were obtained. As expected, two parallel cracks initiated each one from one notch and propagated one after the other. At the end of the test, link-up occurred but it was not symmetric. The first crack had been reoriented toward the beginning of the second one, instead of both cracks propagating up to joining themselves.

In terms of loading, it is concluded from Fig. 12 that the control signal globally followed the elastic loading-unloading from the beginning to the end of the test, even though some offsets and drifts appeared. First, for a control displacement equal to zero, F_Z was equal to about 2.5 kN at the beginning of steps 1, 2 and 3 (respectively periods ($[1,680 - 10,000]$ s, $[10,000 - 18,000]$ s and $[18,000 - 23,000]$ s). Since this value first appeared at the end of elastic unloading, it was assumed that it was generated by a repositioning of the experimental setup during elastic loading-unloading. It thus did not disqualify the test as long as it was taken into account as pre-load. Second, during the steps 1 and 2, the U_Z^{DIC} translation was not exactly equal to zero. Meanwhile, the U_Y^{DIC} translation was higher than the control signal U_Y^{com} during step 1. These differences came from the slight compliance of the setup holding the control cameras.

17

The applied forces and torques moved the cameras a few micrometers away, which induced spurious displacements. The test was however satisfactory. The out-of-plane motions were very small and the related forces even more, and the in-plane displacement field was captured by DIC. These two combined features allow for a posteriori numerical simulations of an in-plane problem.
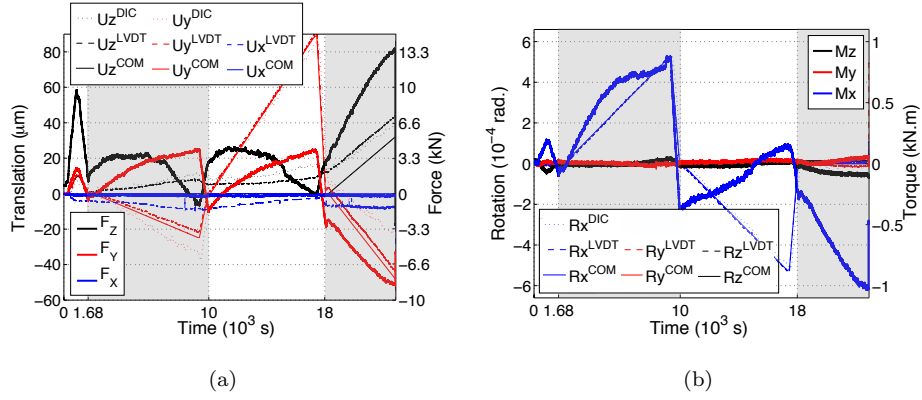

Figure 12: Translation and force curves vs. time (a). Rotation and torque vs. time (b) for $IT2$ test. The first crack initiated after 5,500 s, and the second after 13,500 s (steps are marked by white and light gray backgrounds).

The similarity of steps 2 and 3 is noticeable. First, the symmetry of the two cracks at the end of step 2 is striking. The fact that their propagation length was very close was due to the fact that each step was stopped for the same crack length, which was assessed by DIC during the test. The initial stiffness (Fig. 12(a)) was very close in both cases, and the subsequent decrease of the F_Y and F_Z forces was alike. This similarity was due to the successful closure of the first initiated crack (see Figs. 13 and 14) at the end of step 2. The displacement field where the first crack was located was very smooth, nearly as if no crack had initiated. The fact that the F_Z force tended toward zero when the displacements and M_X torque magnitudes were maximum for both steps (respectively at ca; 9,400 s and 17,200 s) did not mean that the crack completely propagated through the specimen (as confirmed by the displacement

18

fields shown in Figs. 13 and 14), but that the 'compressive' stress σ_{ZZ} on one side of the ligament exactly compensated the 'tensile' stresses of the other side. Both steps ended with a quick unload (ca. 600 to 800 s).
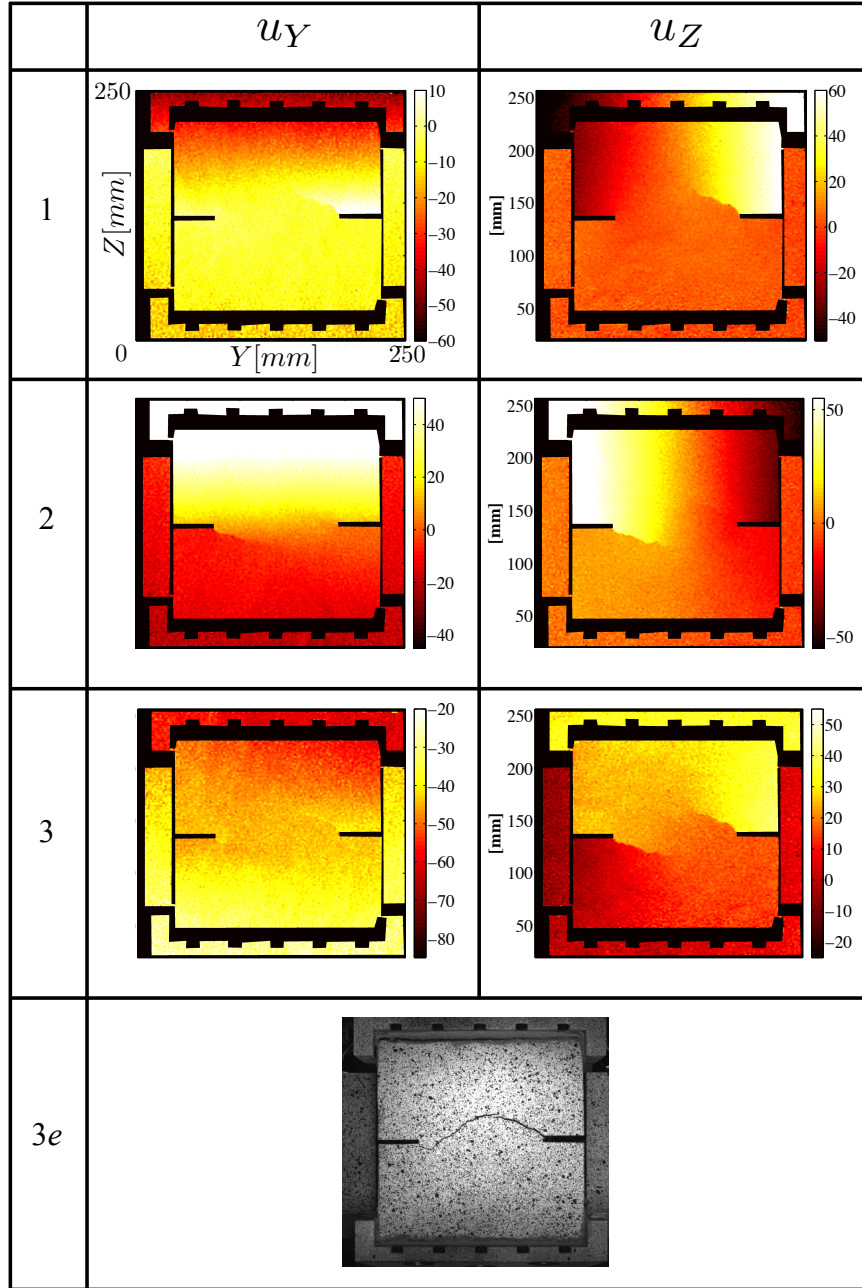
Figure 13: Displacement fields (expressed in μm) on face 1 at the end of step 1 (1), step 2 (2), during step 3 (3) for test *IT2*. The first crack initiated after 5,500 s and the second after 13,500 s. Final macroscopic crack at the end of step 3 (3e).
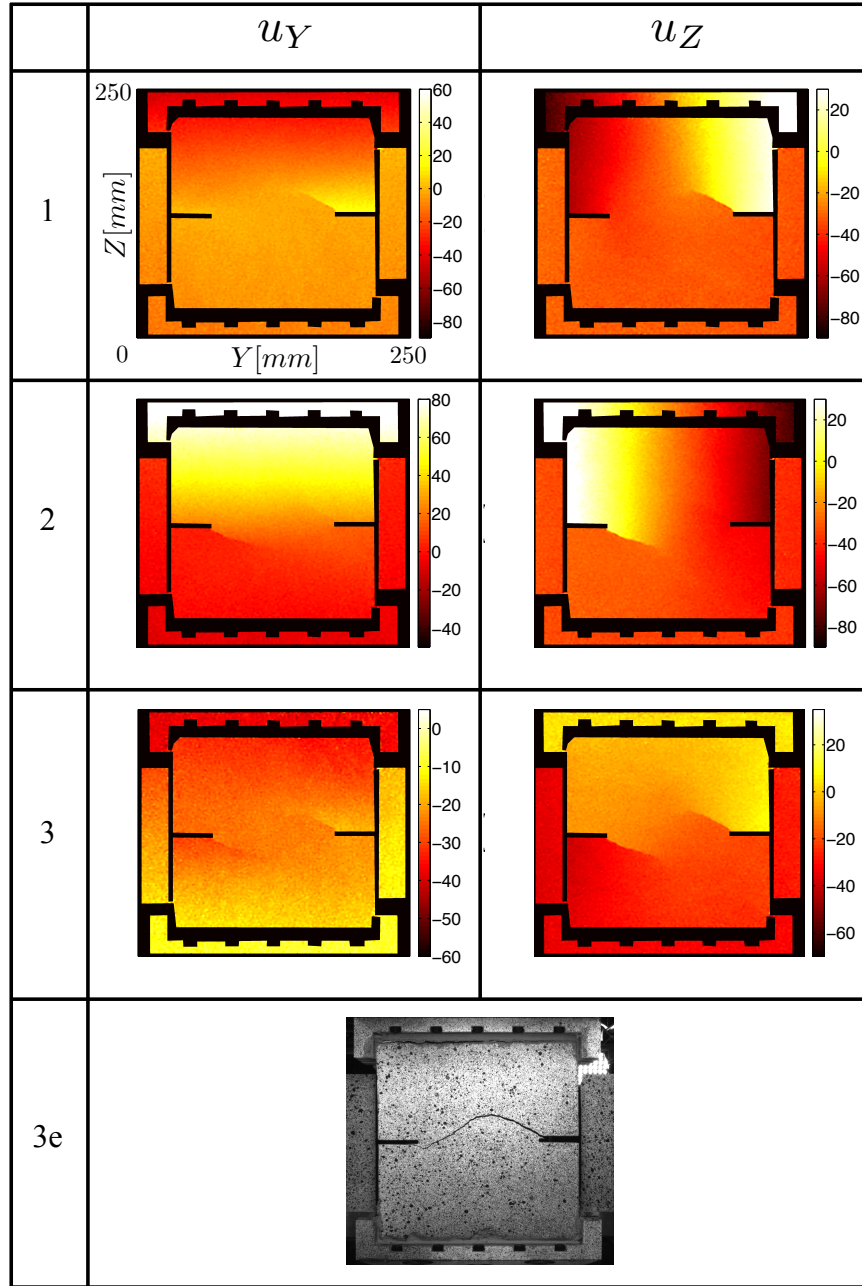
Figure 14: Displacement fields (expressed in μm) on face 2 at the end of step 1 (1), step 2 (2), and during step 3 for test $IT2$. Final macroscopic crack at the end of step 3 (3e). Face 2 images are flipped to make the comparison easier.

The propagation was stable during steps 1 and 2, but not during step 3. For this last step, the displacement was increased slowly, damaging the specimen (the force and torque slopes decreased slightly prior to the sudden failure). The maximum opening of both cracks prior to the propagation is labelled (3) in Figs. 13 and 14. Right after this time step, sudden propagation of the first crack occurred, leading to the final crack depicted with label (3e) in Figs. 13 and 14. Based on the this experimental result, two scenarios may be considered: (1) the lower crack has branched near the notch and propagated in an unstable manner up to the tip of the upper crack, or (2) unstable propagation had started from the upper crack tip and ended in the lower crack, but not at its tip.

4.3. Test IT3

This complex test is only briefly described hereafter since it has been the scope of a dedicated paper, where an in-depth analysis can be found [20]. The overall results were positively satisfactory. The loading was chosen to offer several specific possibilities of crack path and the final crack path corresponded to one of them. A first reorientation instead of branching (see row labelled (3) in Figs. 15 and 16), then a branching instead of a reorientation (row labelled (5)). The displacements and forces (Fig. 17) showed that the case can be considered as an in-plane test, which was confirmed by the very similar displacement fields obtained on each face.
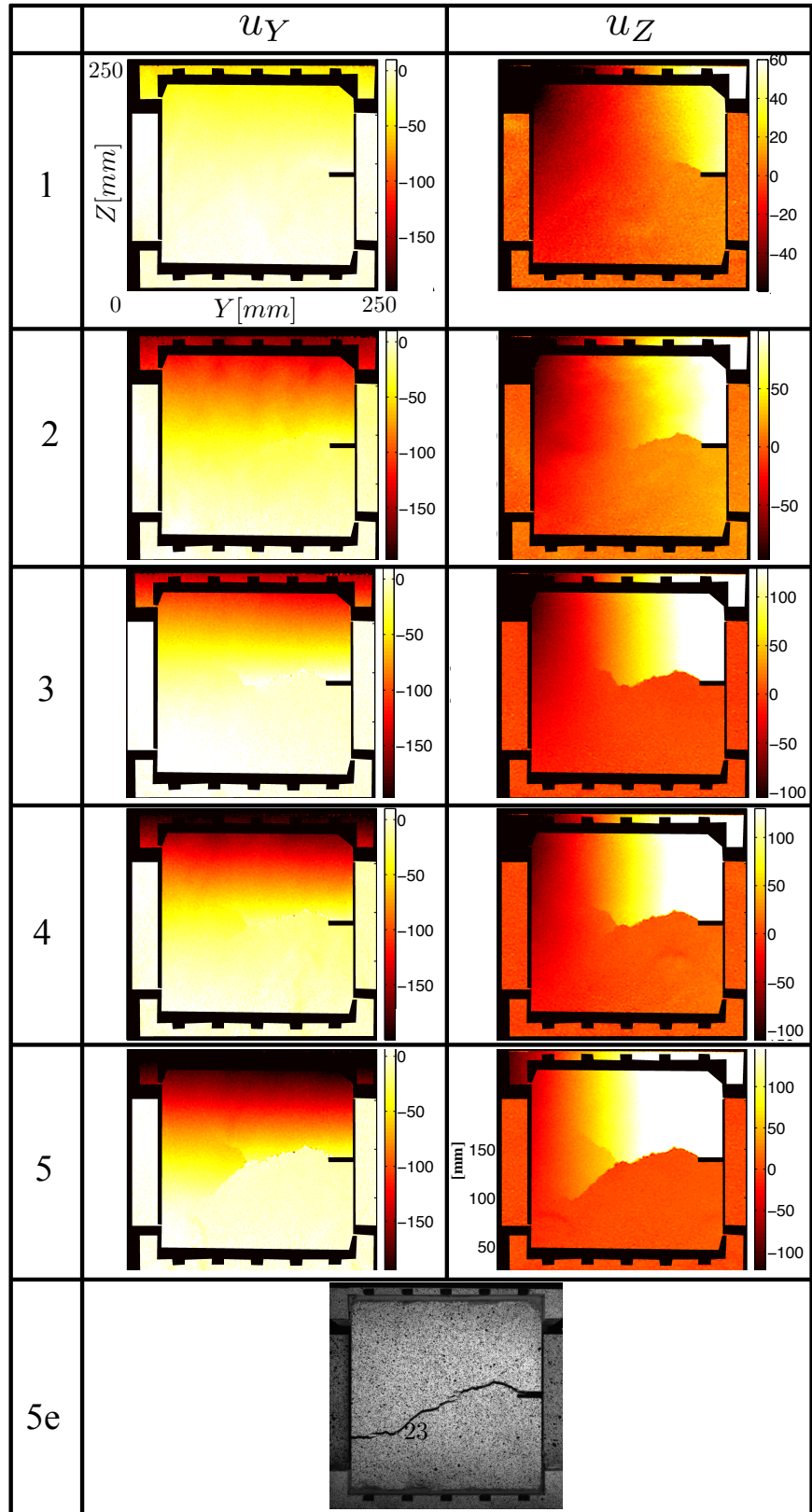
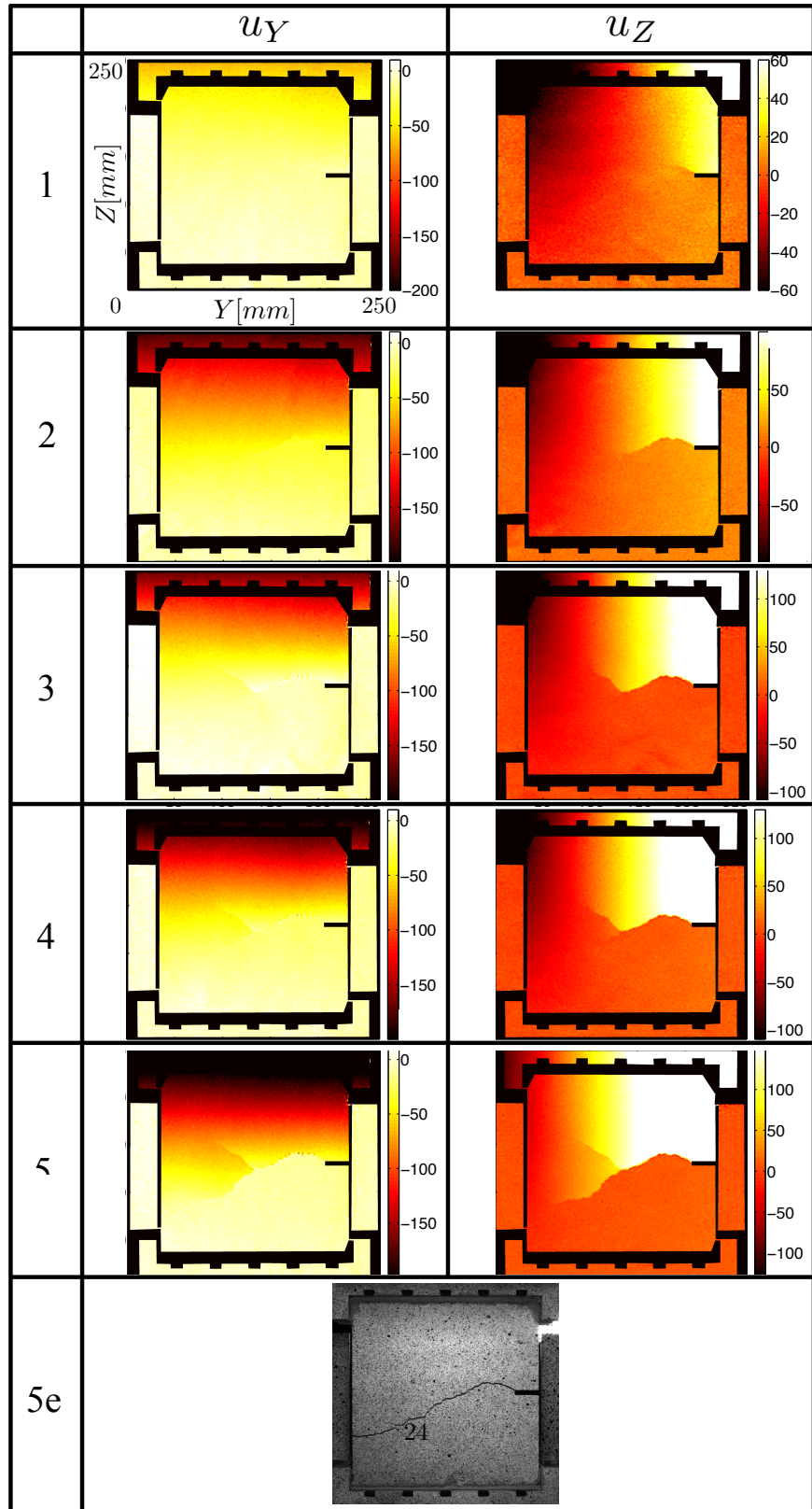Figure 15: Displacement fields (expressed in μm) on face 1 at the end of steps 1 to 5 for test *IT3*.

Figure 16: Displacement fields (expressed in μm) on face 2 at the end of steps 1 to 5 for test $IT3$. Face 2 images are flipped to make the comparison easier.
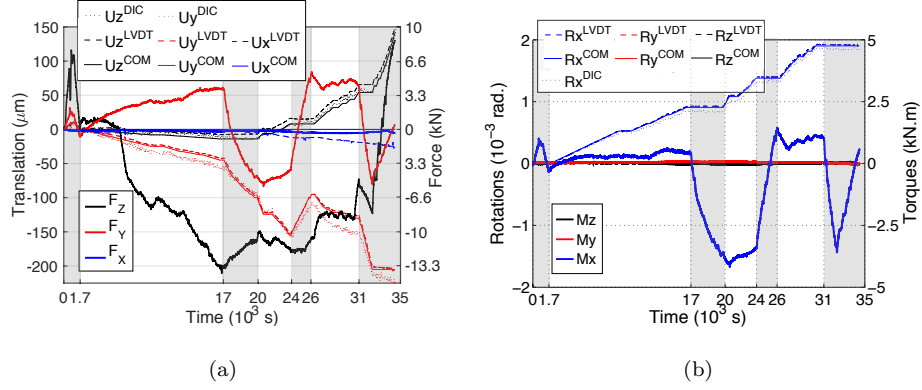
Figure 17: Translation and force vs. time (a). Rotation and torque vs. time (b) for $IT3$ test (steps are marked by white and light gray backgrounds).

Concerning the propagation history, several plateaus are visible in Fig. 17, which were due to the fact that the applied displacements were stopped while the location of the crack tip was assessed by DIC. Only the final crack propagation was unstable. It is worth noting that crack propagation was stable and gradual all along the duration of the test. The crack initiated at about $t = 6,000$ s, and propagation occurred during steps 1, 3, 5 and 7 (resp. $[1,700 - 16,000]$ s, $[20,000 - 23,000]$ s, $[25,000 - 30,000]$ s and $[32,000 - 35,000]$ s periods), but not during the reorientation steps 2, 4 (resp. $[16,000 - 20,000]$ s, $[23,000 - 25,000]$ s periods). Conversely, the crack propagated slightly downward with a branching phenomenon during reorientation step 6. F_Y tended to zero because of the thinning of the ligament. The $F_Z(U_Z)$ slope (Fig. 18(a)) was lower than at step 0, thereby proving that the load was (mainly) transmitted through the ligament.
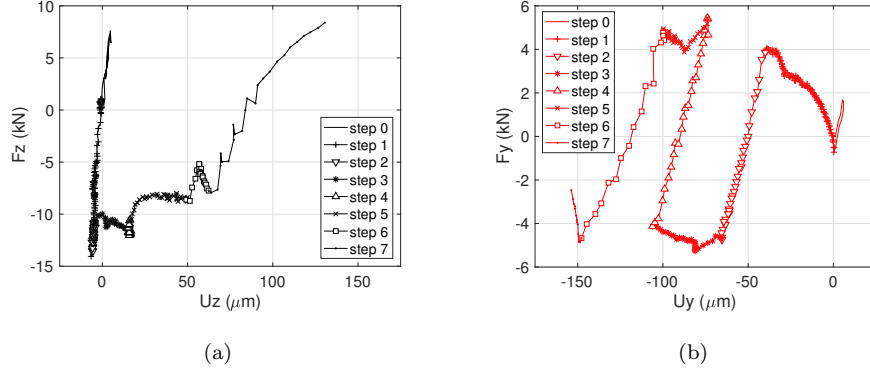
25

Figure 18: F_Z force versus U_Z translation (a). F_Y force versus U_Y translation during $IT3$ test.

Despite an increasing crack opening, the load was still transmitted through the crack faces during the majority of the test. The average stiffness along $\underline{Y}$ (*i.e.,* the slope of F_Y vs. U_Y, see Fig. 18(b)) was virtually identical for the elastic loading and steps 2, 4, and even at the beginning of step 6. No progressive increase of stiffness was observed due to slow crack closure during these steps. It may be concluded that even if the (normal) crack opening was important, up to 50 (resp. 75) μm during step 2 (resp. 4), there still was (lateral) contact due to the crack roughness, except during step 6.

4.4. Test IT4

This last more 'exotic' test tried to propagate a crack in mixed-mode I-II, and then in mixed-mode I-III. Because of its complexity, this test is not specifically intended for experimental-numerical comparison, but for proving that it can be conducted with such setup. The mixed-mode I-II loading is shown Fig. 19.
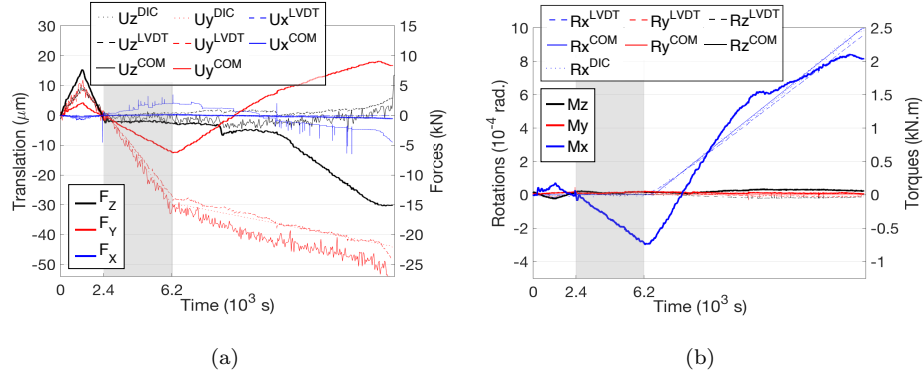
26

Figure 19: Translation and force vs. time (a). Rotation and torque vs. time (b) for the first part of $IT4$ test (steps are marked by white and light gray backgrounds).

It consisted of 3 steps, namely, first an elastic loading-unloading $I0$ sequence, then a first shear $I1$, and last a shear-rotation combination $I2$. The nonlinear change of F_Y, F_Z and M_X while the prescribed displacement was linear proved that the loading induced an initiation and propagation of a crack during this last step. It stopped at approximately mid-width of the specimen at the end of step $I2$ (see Figs. 20 and 21). The crack had equally propagated on each face with the same orientation, and the forces had significantly decreased, meaning that the crack also propagated through the bulk.
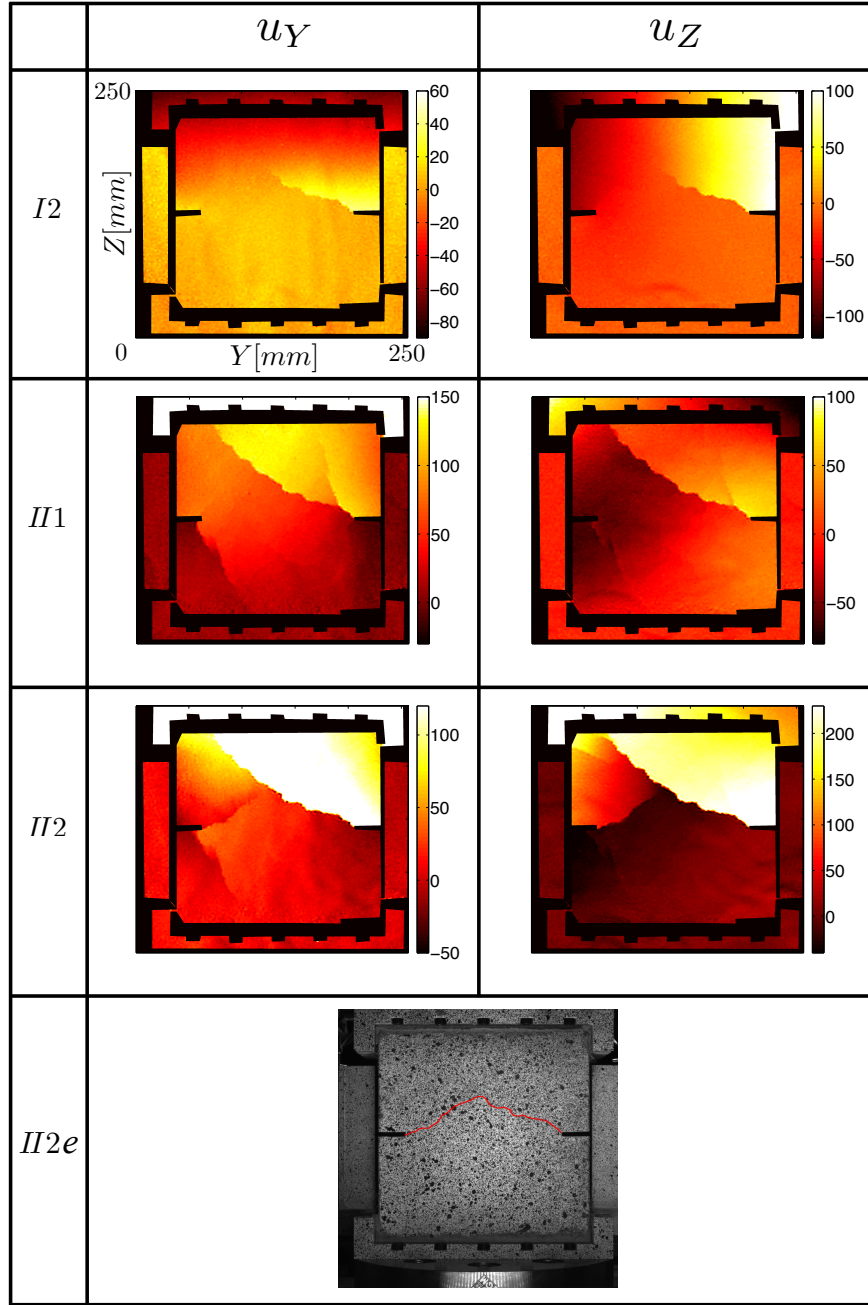
27

Figure 20: Displacement fields (expressed in μm) on face 1 at the end of steps $I-2$, $II-1$ and $II-2$ for test $IT4$. Final main crack is highlighted in red because the final opening is barely visible on the image.

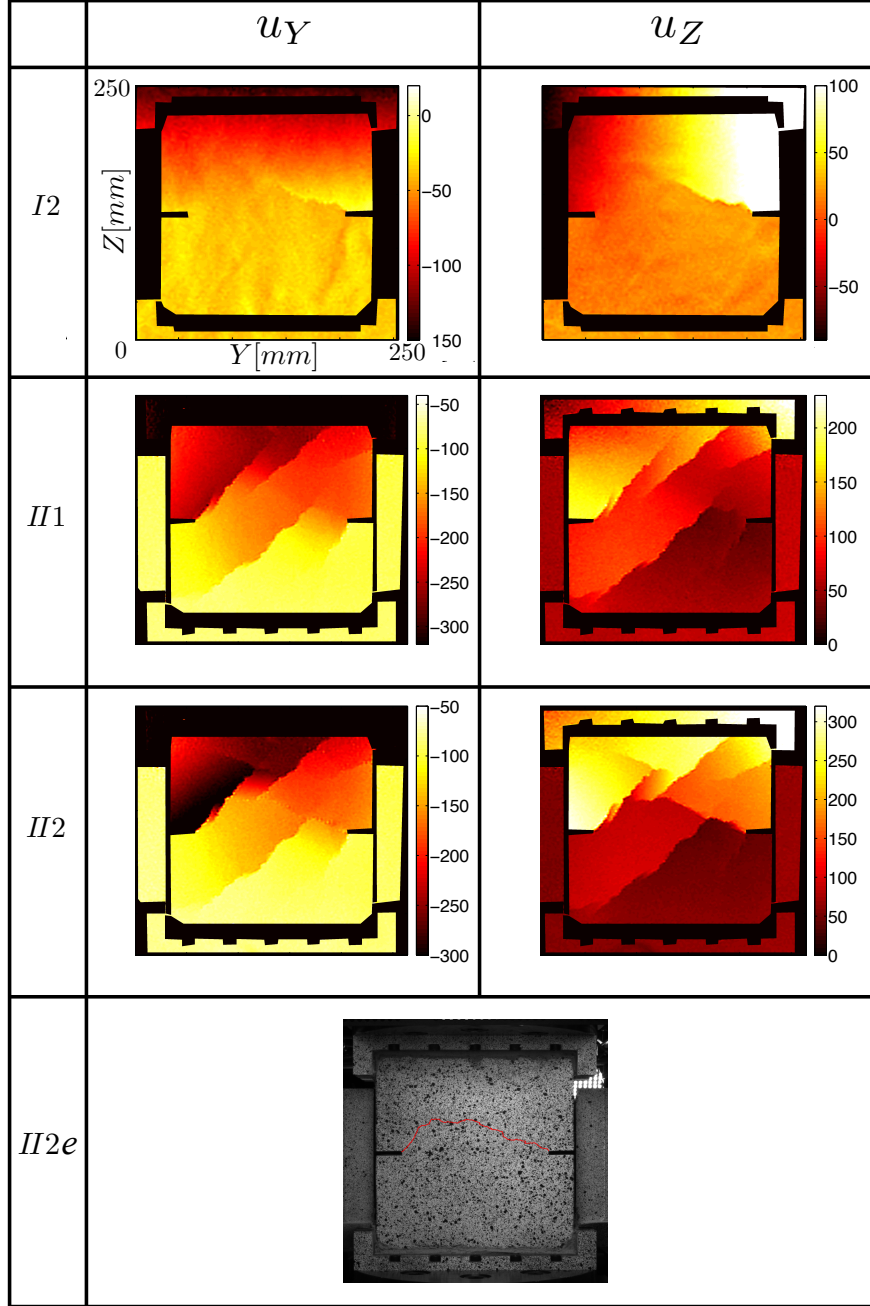Figure 21: Displacement fields (expressed in μm) on face 2 at the end of steps $I-2$, $II-1$ and $II-2$ for test $IT4$. Face 2 images are flipped to make the comparison easier. Final main crack is highlighted in red because the final opening is barely visible on the image.

The second part was simple in terms of prescribed displacement (Fig. 22). A first step $II1$ was a R_Z rotation while the second step $II2$ was a U_Z translation.

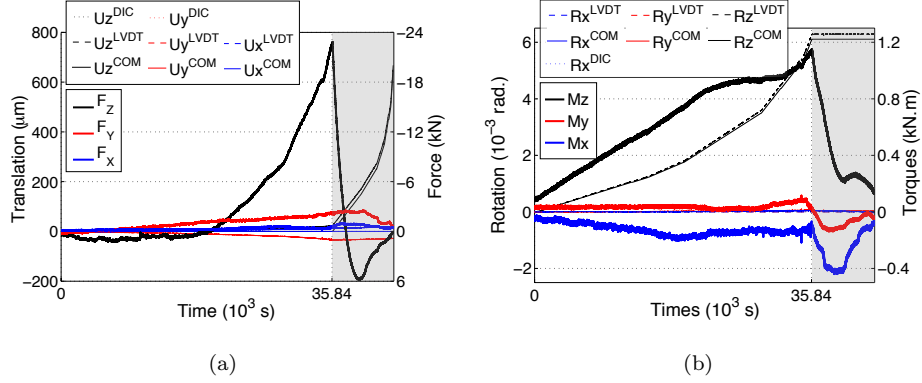(a)   (b)

Figure 22: Translation and force vs. time (a). Rotation and torque vs. time (b) for the second part of $IT4$ test. The force axis is inverted for a better visibility (steps are marked by white and light gray backgrounds).

335   The result turned out to be more complex than expected. During step $II1$ the existing crack on face 1 (Fig. 20) propagated because its orientation matched the natural tendency to grow. Conversely, on face 2 (Fig. 21) the original crack did not grow because the mode III loading induced its closure. Aside from the propagation of the original crack, it was noticed that additional cracks initiated 340   and propagated on both faces to adapt the large prescribed rotation. Figure 20 shows that one crack initiated from each of the notches on face 1, while on face 2 (Fig. 21), 7 appear with 2 initiating from the notches. Other cracks started from the U-shape plates or from no particular location of face 1. Despite the numerous visible cracks, an important load level was still measured at the end 345   of the first step $II1$ (Fig. 22) probably because of a 'jamming' phenomenon, and the fact that the cracks were not all transverse through the bulk. By applying the last U_Z translation during step $II2$, existing cracks opened even more while new cracks appeared, thereby creating a complex network. The load decreased during this last step, down to complete failure.

30

5. Conclusion

This paper presented a series of 4 crack propagation tests on identical compact mortar specimens. The setup was identical to that used in so-called proportional and non-proportional tests [1]. However the loading history was now enriched with rotations, which led to important improvements in two different domains.

From the experimental techniques point of view, several points are noticeable. First, it was proven that in-plane rotations helped stabilize crack propagation, or control the propagation of 2 different cracks. Consequently, the tests were richer because the information can be acquired during the whole propagation steps contrary to an early unstable propagation [1]. Second, the loadings with additional rotation induced crack propagations through the material bulk, contrary to the non-proportional loadings only relying on two translations [1]. The displacements measured by DIC on both faces was thus meaningful from the mechanical standpoint, thereby enabling for experimental-numerical comparisons. Third, the crack tip position was evaluated during the tests with full-field measurements in order to reorient it by changing the loading history. Studies of crack reorientation or branching are thus possible. Last, since the testing machine had 6-axes, mode III was also presented as a proof of the versatility of the whole setup. The gathering of all these different enhancements (*i.e.,* stability, versatility, interactivity) pave the way for rich hybrid test generations [19].

For model identification and validation purposes, the results of this series of tests constitute a rich database (data of tests *IT*1 *IT*2 and *IT*3 are available online (`https://doi.org/10.5281/zenodo.2625006`). The propagation of cracks was extensively monitored for all the reported tests, as well as the overall force and torque history, which enable for thorough experimental/numerical comparisons. With the chosen loading paths and observed crack paths, these data are an interesting challenge for damage and fracture models, in particular the prediction of reorientation, branching, instability and crack arrest.

To this aim, the measured data of $IT2$ and $IT3$ tests were used in the so-called CARPIUC Benchmark [25] of CFRAC 2017 and CFRAC 2019 conferences (the benchmark data can be found online[1]) in which several teams participated [26, 27, 28, 29, 30, 31, 32].

Last, these complex tests (*i.e.,* based on a combination of multiaxial loading conditions and full-field measurements) relying on an interactive procedure (*i.e.,* the decision to change or not, and to which extent, the orientation of the crack at each step of the test) pave the way for future hybrid tests [19], which are driven 'on the fly' by computed quantities.

Acknowledgements

References

[1] A. Carpiuc-Prisacari, C. Jailin, M. Poncelet, K. Kazymyrenko, H. Leclerc, F. Hild, Experimental database of mixed-mode crack propagation tests performed on concrete specimens with a hexapod and full-field measurements. Part I: predefined loading (submitted for publication).

[2] M. Nooru-Mohamed, Mixed-mode fracture of concrete: an experimental approach, Ph.D. thesis, Technische Universiteit Delft. (1992).

[3] M. B. Nooru-Mohamed, E. Schlangen, J. G. M. van Mier, Experimental and numerical study on the behavior of concrete subjected to biaxial tension and shear, Advanced Cement Based Materials 1 (1) (1993) 22–37.

[4] N. Iosipescu, New accurate procedure for single shear testing of metals, Journal of Materials 2 (1967) 537–566.

---

[1]https://figshare.com/s/b1177c9317bcc0710521

[5] M. Arrea, A. Ingraffea, Mixed mode crack propagation in mortar and con-
crete, Tech. Rep. 81-13, Department of Structural Engineering, Cornell
University (1982).

[6] Z. Bažant, P. Pfeiffer, Shear fracture tests of concrete, Materials and Struc-
tures 19 (1986) 111–121.

[7] L. Biolzi, Mixed mode fracture in concrete beams, Engineering Fracture
Mechanics 35 (1990) 187–193.

[8] S. Swartz, M. Taha, Mixed mode crack propagation and fracture in con-
crete, Engineering Fracture Mechanics 35 (1990) 137–144.

[9] E. Ballatore, A. Carpinteri, G. Ferrara, G. Melchiorri, Mixed mode fracture
energy of concrete, Engineering Fracture Mechanics 35 (1-3) (1990) 145–
157.

[10] P. Bocca, A. Carpinteri, S. Valente, Mixed mode fracture of concrete, In-
ternational Journal Solids and Structures 27 (1991) 1139–1153.

[11] E. Schlangen, J. V. Mier, Mixed-mode fracture propagation: a combined
numerical and experimental study, Fracture and Damage of Concrete and
Rock (1993) 166–175.

[12] D. Brokenshire, Torsional fracture tests, Ph.D. thesis, Cardiff University
(1996).

[13] B. Winkler, Traglastuntersuchungen von unbewehrtenund bewehrten Be-
tonstrukturen, Ph.D. thesis, University of Innsbruck (2001).

[14] J. Galvez, M. Elices, G. Guinea, J. Planas, Mixed mode fracture of concrete
under proportional and nonproportional loading, International Journal of
Fracture 94 (1998) 267–284.

[15] M. Nierenberger, M. Poncelet, S. Pattofatto, A. Hamouche, B. Raka, J. M.
Virely, Multiaxial testing of materials using a stewart platform: Case study
of the nooru-mohamed test, Experimental Techniques 38 (2) (2012) 74–83.

33

[16] J. Le Flohic, V. Parpoil, S. Bouissou, M. Poncelet, H. Leclerc, A 3D displacement control by digital image correlation for the multiaxial testing of materials with a Stewart platform, Experimental Mechanics 54 (5) (2014) 817–828.

[17] Z. Tomičević, F. Hild, S. Roux, Mechanics-aided digital image correlation, Journal of Strain Analysis for Engineering Design 48 (2013) 330–343.

[18] J. G. M. van Mier, M.B. Nooru-Mohamed, Geometrical and structural aspects of concrete fracture, Engineering Fracture Mechanics 35 (4-5) (1990) 617–628.

[19] C. Jailin, A. Carpiuc, K. Kazymyrenko, M. Poncelet, H. Leclerc, F. Hild, S. Roux, Virtual hybrid test control of sinuous crack, Journal of the Mechanics and Physics of Solids 102 (2017) 239–256.

[20] A. Carpiuc-Prisacari, M. Poncelet, K. Kazymyrenko, H. Leclerc, F. Hild, A complex mixed-mode crack propagation test performed with a 6-axis testing machine and full-field measurements, Engineering Fracture Mechanics 176 (2017) 1–22.

[21] AFNOR, Méthodes d'essais des ciments - Partie 1 : détermination des résistances mécaniques (NF EN 196-1) (april 2006).

[22] RILEM TCS, Determination of the fracture energy of mortar and concrete by means of three-point bend tests on notched beams, Materials and Structures 18 (106) (1985) 285–290.

[23] B. Beaubier, J. Dufour, F. Hild, S. Roux, S. Lavernhe, K. Lavernhe-Taillard, CAD-based calibration and shape measurement with stereoDIC - principle and application on test and industrial parts, Experimental Mechanics 54 (3) (2014) 329–341.

[24] J.-E. Dufour, B. Beaubier, F. Hild, S. Roux, CAD-based displacement measurements with stereo-DIC. Principle and first validation, Experimental Mechanics 55 (9) (2015) 1657–1668.

[25] A. Carpiuc, M. Poncelet, J. Réthoré, S. Roux, CARPIUC Benchmark. crack advance, reorientation, propagation and initiation under complex loadings, Advanced Modeling and Simulation in Engineering Sciences 5 (2018) 1–24.

[26] C. Oliver-Leblond, Beam-particle approach to model the quasi-brittle behaviour of concrete. carpiuc benchmark, in: Book of abstracts of CFRAC 2017 International Conference on Computational Fracture and Failure of Materials and Structures, 2017, pp. 319–320.

[27] E.Delaume, L.Daridon, Y.Monerie, F.Dubois, F.Perales, Local adaptive refinement method applied to cohesive zone models for heterogeneous materials, in: Book of abstracts of CFRAC 2017 International Conference on Computational Fracture and Failure of Materials and Structures, 2017, pp. 321–322.

[28] T. Nguyen, J. Réthoré, J. Yvonnet, M.-C. Baietto, A phase field method for modelling of crack propagation and initiation under complex loadings, in: Book of abstracts of CFRAC 2017 International Conference on Computational Fracture and Failure of Materials and Structures, 2017, p. 324.

[29] J. Ŏzbolt, J. Bŏsnjak, A. Sharma, Modelling mixed mode fracture of cementitious materials using microplane model with relaxed kinematic constraint - carpiuc benchmark, in: Book of abstracts of CFRAC 2017 International Conference on Computational Fracture and Failure of Materials and Structures, 2017, p. 323.

[30] A. Salzman, N. Chevaugeon, N. Moës, Simulation of the carpiuc test with the thick level set model, in: Book of abstracts of CFRAC 2017 International Conference on Computational Fracture and Failure of Materials and Structures, 2017, p. 327.

[31] T. Wu, A. Carpiuc-Prisacari, M. Poncelet, L. De Lorenzis, Phase-field simulation of interactive mixed-mode fracture tests on cement mortar with full-field displacement boundary conditions, in: Book of abstracts of CFRAC

2017 International Conference on Computational Fracture and Failure of Materials and Structures, 2017, p. 325.

[32] A. Carpiuc, K. Kazymyrenko, M. Poncelet, F. Hild, Non-local damage model to simulate the quasi- brittle behaviour of concrete carpiuc benchmark, in: Book of abstracts of CFRAC 2017 International Conference on Computational Fracture and Failure of Materials and Structures, 2017, p. 326.

490